Silicon
https://doi.org/10.1007/s12633-023-02332-7

ORIGINAL PAPER

Effect of green synthesis bimetallic Ag@SiO_2 core–shell nanoparticles on absorption behavior and electrical properties of PVA-PEO nanocomposites for optoelectronic applications

Ehssan Al-Bermany[1] · Ali Tao'mah Mekhalif[2] · Hikmat A. Banimuslem[2] · Karar Abdali[3] · Mohammed M. Sabri[4]

Received: 15 September 2022 / Accepted: 3 February 2023

Abstract
A green and easy technique was used to synthesize silver and silica (Ag@SiO_2) core–shell nanoparticles (NPs) in the matrix blend polymers matrix. Core–shell nanoparticles were loaded into polyvinyl alcohol (PVA) and ultrahigh molecular weight polyethylene oxide (UHMW-PEO) blended polymer to fabricate new nanocomposite films (NCFs) using the developed solution-sonication-casting technique. The spectroscopic properties of the resultant films were investigated using x-ray diffraction (XRD), Fourier transforms infrared (FTIR), visible light microscope (OLM), field emission scanning electron microscope (FESEM), FESEM-energy dispersive spectroscope (FESM-EDX), UV/visible spectrometer, and LCR meter to investigate the structural, morphological, optical, and electrical characteristics. XRD revealed the presence of the semi-crystalline nature of PVA-UHMWPEO/ Ag@SiO_2 NCFs. The degree of crystallinity increased after embedding. The NPs were well distributed within the NCFs according to OLM and SEM, and FESM-EDX confirmed the presence of C, O, Si, and Ag elements. FTIR spectrum observed strong bonding after the loading of NPs, and other peaks were hidden. The UV/visible spectrums suggested an absorption at ~ 210 nm. Based on the Tauc plot model, the optical bandgap (Eg) values decreased from 5.52 eV to 4.57 eV. The electrical conductivity values were significantly increased with the increasing frequency and (Ag@SiO_2) core–shell nanoparticles (NPs) loading ratio. The PVA-UHMWPEO/Ag@SiO_2 NCFs explained enhanced lattice strain. The obtained NCFs are suitable for use in various optoelectronic and nanodevice applications.

Keywords PVA/UHMWPEO · Ag@SiO_2 · Core–shell nanoparticles · Nanocomposites

1 Introduction

Mixing two or more polymers is very significant for getting a novel or hybrid material suitable for a wide range of applications [1]. Hybrid polymer blends (HPB) can enable more effortless casting and primary treatment with nanofillers to prepare new nanocomposite films (NCFs) as per their structural, morphological, optical, and electrical characteristics [2]. Incorporating nanoparticles (NPs) into the polymer blend gives suitable properties for modern applications [3]. NCFs based on HPB with NPs have been studied due to their increasing characteristics that improve the interfacial interaction between these compositions [4]. The NCFs show enhanced structural, morphological, optical, and electrical properties [5]. Nowadays, nanotechnology (NT) has a considerable concern in several fields because the materials at the nanoscale have novel and enhanced chemical, optical, electrical, and optoelectronic properties [6]. Various photochemical and chemical methods can synthesize NPs. Researchers have been using metallic NPs for years, intensely employed in sensors, nano-devices, optoelectronics, and medical sciences [7]. Herein, the attention concentrated on bimetallic instead of one-metal NPs due to their novel characteristics and because they are more applicable and cheaper than other NPs [8].

Polyvinyl alcohol (PVA) is a thermoplastic polymer synthesized from the hydrolysis of polyvinyl acetate [8]. It is

✉ Ehssan Al-Bermany
ehssan@itnet.uobabylon.edu.iq

1 Physics Department College of Education for Pure Sciences, University of Babylon, Babylon, Iraq

2 Physics Department College of Science, University of Babylon, Babylon, Iraq

3 Iraq Ministry of Education, Baghdad, Iraq

4 Department of Physics Faculty of Science and Health, Koya University, Koya KOY45 Kurdistan Region F. R, Erbil, Iraq

Published online: 09 February 2023

well-soluble in water and used in different medical, industrial, optoelectronic, and other applications [9]. PVA can easily and rapidly combine with other materials to form blends or composites [10]. Polyethylene oxide (PEO) is a semicrystalline and water-soluble polymer [11]. PEO widely use in medical, cosmetics, electronic industries, and optoelectronic purposes because of its novel characteristics [12, 13].

The optical properties of polymers increase the knowledge of the polymer's internal structure and the bonds' nature and broaden the horizon of potential use areas [14]. In order to determine the many optical properties of different ranges of wavelengths, it is necessary to know the absorption, polymer's absorption, reflectivity, and transmittance spectra of the bonds, energy rays, and orbitals can be deduced by studying the ultraviolet (UV) spectrum. Therefore, studying the visible spectrum provided sufficient information about the material's behavior for several applications, such as electro-optic and solar energy applications. The electrical can be defined as the charge unit's movement is known as charge carriers, which is focused on the potential difference effect. Polymers are not completely free of conduction processes, and many charge carriers may possess low-level conduction. The ability of electrical conductivity of matter can be categorized as the materials to insulators, semiconductors, conductors, and superconductive [15]. The electrical properties of the material are determined not only by chemical composition but also by the arrangement of atoms in the solid and the existence of defects when giving rise to the electron states in the energy gap. Can be reduced this defect by different processes, such as the annealing process. The electrical properties highly depend on the preparation technique and the deposition conditions [16].

Several types of research [17–21] use different methods to synthesize silver (Ag) with silicon oxide (SiO_2) using different procedures and techniques for various applications. Asselin et al. [20] tried to control the core size and silica spacer shell thickness of synthesized Ag@SiO_2 with fluorescein, eosin, or rhodamine B nanostructures using chemical methods. They focused on the effect of the core shell on fluorescence emission intensity, characterized by transmission electron microscopy, UV–VIS spectrometry, time-resolved fluorometry, and spectrofluorimetry. The results showed critical parameters for designing colloidal sensors for the future generation of metal-enhanced fluorescence (MEF) sensors. Wang et al. [21] coated the silver with SiO_2 as a core–shell microstructure using a reverse micelle technique. They used various particle sizes smaller than 50 nm. They reported good agreement between the theoretical and experimental results of the refractive indices. They also investigated the size of the silver quantum dot, color change, which they observed redshift, and optical absorption around 410 nm of the Ag@SiO_2 nanocomposites. Liang et al. [22] used a facile sol–gel process and heat treatment to synthesize SiO_2@YVO_4:Yb^{3+} and an Er^{3+} core–shell structure. They reported the successful coating of YVO_4:Yb^{3+} and Er^{3+} of SiO_2 as core–shell structures, where the samples displayed under the excitation of a 980 nm laser diode a bright green luminescence and photoluminescence intensity improved with increasing the coating number, which showed great potential for infrared detection and optical devices. Ag@SiO_2 are advanced experimental materials used primarily as encapsulated materials for different polymer types due to their high individual surface zone, distribution, high purity, and simplicity of use [18, 23]. Ag@SiO_2 has recently attracted good attention for its use in an enormous range of electronic and photonic applications [17, 23, 24].

Recent publications reported several methods to syntheses or control the particle size of Ag@ SiO_2 core–shell, such as using chemical processes to control the core size and silica spacer shell thickness of synthesized Ag@SiO_2 [20], a reverse micelle technique by coating the silver with SiO2 as a core–shell microstructure [21], a facile sol–gel process and heat treatment to the coating of YVO4:Yb3 + and Er3 + of SiO_2 as core shell structures [22]. Most previous publications focused on the independent preparation of core shells, such as Cu@Ag [25] or Ag@ SiO_2 [18–22], then characterized their properties as nanoparticles. Whereas this study used different technical totally that focused on developing new and green methods to obtain Ag@SiO2 core shell nanoparticles through loading and mixing the Ag with blended polymers, they were then loaded with different rations of SiO_2 to surround the Ag inside the polymers matrix and then getting PVA-PEO/Ag@ SiO_2 as nanocomposites.

Recent publications reported several methods to syntheses or control the particle size of Ag@SiO_2 core–shell, such as using chemical processes to control the core size and silica spacer shell thickness of synthesized Ag@SiO_2 [20], a reverse micelle technique by coating the silver with SiO_2 as a core–shell microstructure [21], a facile sol–gel process and heat treatment to the coating of YVO_4:Yb^{3+} and Er^{3+} of SiO_2 as core shell structures [22]. Most previous publications focused on the independent preparation of core shells, such as Cu@Ag [25] or Ag@SiO_2 [18–22], then characterized their properties as nanoparticles. Whereas this study used different technical totally that focused on developing new and green methods to obtain Ag@SiO_2 core shell nanoparticles through loading and mixing the Ag with blended polymers, then loaded of different rations of SiO_2 to surround the Ag inside the polymers matrix and then getting PVA-PEO/Ag@SiO_2 as nanocomposites.

Additionally, despite the several recent publications to fabricate Ag@SiO_2 core–shell nanoparticles using chemical or complex techniques, this study's essential aim is to use green and easy solution-sonication-casting methods to synthesize Ag@SiO_2 core–shell nanostructure and investigate their impact on the structural, morphological, optical, and

electrical properties of blended polymer PVA-PEO/Ag@SiO_2 nanocomposites and the ability to use them in various optoelectronic devices.

2 Practical Section

2.1 Materials

PVA $(-CH_2CHOH-)_n$ with M_w of 160 kg.mol^{-1} from Media Labs Pvt. Country, UHMW-PEO $(-CH_2CH_2O-)_n$ with $M_w \sim 5{,}000{,}000$ kg.mol^{-1}, silica NPs with an average grain size of between 20 and 30 nm from Sigma Aldrich, the UK, and silver NPs from Sky Spring NMs, Country, with a 20 to 30 nm average grain.

2.2 Purification of the NCFs

Firstly, 0.8 g of PVA and 0.2 g of UHMWPEO were independently dissolved in deionized water using a magnetic stirrer (Stuart stirrer) and sonication bath (VG-1613QTD, frequency kHz, and Ultrasound power 60W) at room temperature 30 ± 2 °C for 2 h until getting an acceptable homogenous solution. The blended polymer mixture was cast in a Petri dish and left to dry for 6 days under air at room temperature, resulting in a blended polymer film. In the progress of generating core–shell structure, different amounts of Ag@SiO_2 NPs were loaded independently. Briefly, one loading ratio of Ag (0.015 wt. %), which was loaded in all samples, was first to the PVA-UHMWPEO and then striated for 2 h using a magnetic stirrer. Then SiO_2 with the same loading of (0.015 wt. %) was added to PVA-UHMWPEO/Ag and mixed for 2 h. This ratio of SiO_2 noted has circular shapes, but it was not enough to surround the Ag and get the core–shell structure. Therefore, the loading ratio of SiO_2 was duplicated to 0.030 wt. % and using the same procedure that improved and started to have circles shapes but is still not enough to surround the Ag as core–shell structure. Therefore, the loading ratio was increased again to 0.045 and then 0.060 wt. % until getting the clear Ag nanoparticle surrounded by SiO_2 sample E3 and clearly presents the core–shell structure in sample E4 as shown in OM and FESEM images. The nanocomposite was named E0, E1, E2, E3, and E4, respectively, as shown in Table 1. The thicknesses of the obtained films were evaluated to be between 0.084 and 0.093 cm.

2.3 Techniques

XRD (X-pert) produced by Phillips Co., OLM (Nikon-73,346) spectrometer manufactured by Olympus Co., SEM (Mira-3) system made by T-scan Co., within (1.2 nm at 30 kV) and (2.3 nm at 3 kV), EDX produced by Oxford instrument, FTIR (vertex 70) instrument made by Bruker Co., UV/visible properties were studied by a double beam Shimadzu (1800) spectrometer, and. The AC electrical properties were measured by an LCR meter, Hi TESTER, and HIOKI (3532–50).

Table 1 Summarized the sample preparations

Sample code	Concentration Wt. %			
	PVA	UHMWPEO	AgNPs	SiO_2NPs
E0	0.80	0.200	0	0
E1	0.80	0.170	0.015	0.015
E2	0.80	0.155	0.015	0.030
E3	0.80	0.140	0.015	0.045
E4	0.80	0.125	0.015	0.060

3 Results and Discussion

3.1 Structural Studies

X-ray diffraction spectra for $PVA_{80\%}$-$UHMWPEO_{20\%}$ blended polymer without and with 0.0, 0.015, 0.030, 0.045, and 0.060 wt. % of Ag@SiO_2 (50:50) nanoparticles are exhibited in Fig. 1. The PVA-UHMWPEO pattern showed two peaks at 2θ = 18.76° (120) and 22.78° (112), which are related to UHMWPEO [5]. In contrast, the PVA peak, usually presented at 2θ = 19.9° (101), disappears due to overlapping with the high intensity of UHMWPEO peaks, in agreement with other reports [26, 27]. The incorporation of Ag@SiO_2 revealed that significant peaks are not present in blended polymers (E0), where several peaks presented a Bragg angle at 2θ = 42.81°, 46.20°, and 47.16° correlated to SiO_2, in addition to other peaks at 2θ = 29.25°, 30.51°, 37.94°, 44.29°, 47.16°, and 77.17° associated with Ag [17]. The Bragg angle of both Ag@SiO_2 nanoparticles in the nanocomposites agrees with JCPDS data (card No. 01–086-1561).

It is clear that increasing the loading ratio of nanoparticles associated with broadened the diffraction peaks of the polymers in the matrix, which may be credited to the difference in the degree of deacetylation of PVA- UHMWPEO. Where some peak intensities were significantly reduced, and others increased, this inculcated a change in the crystalline size of polymers, where the crystallite size of polymers decreased with increasing the loading ratio of the Ag@SiO_2 core–shell. Other peaks shifted, such as from 28.70° to 29.25°, or diapered, for instance, 37.56°, as presented in (E4) compared to other samples (E1, E2, and E3) and blended polymers (E0). Results referred to interfacial interaction between the blend and NPs during the formation of the nanocomposite films that led to the partial change of the crystalline size of the polymer [18].

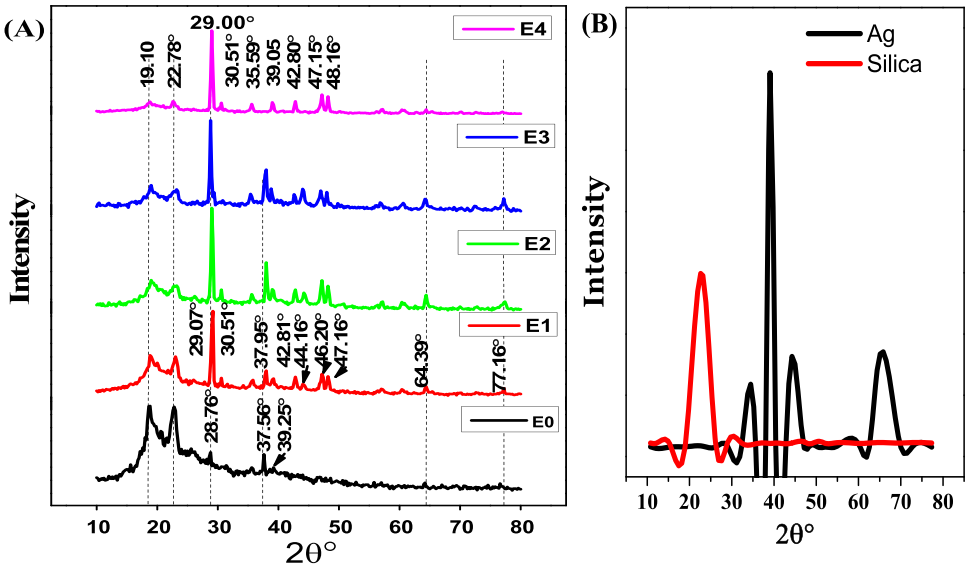

Fig. 1 XRD of prepared of **A**) sample, and **B**) Ag and SiO_2.

From the XRD peak position, several factors could be estimated for a better understating of the XRD results of the samples, where the interplanar d-spacing (d) is calculated using the Bragg equation [28].

$$n\lambda = 2dsin(\theta) \tag{1}$$

(n), (λ), (d), and (Θ) mean the integer, wavelength, and angle of the X-ray between the incident and scattering beam, respectively. Meanwhile, the crystallite size (D nm) is calculated by applying the Scherrer formula (2) [29].

$$D = k\lambda/\beta\cos(\theta) \tag{2}$$

($k = \sim 0.9$) is the factor of the crystals mean and (β) the full width at half the maximum peak (FWHM), as exposed in Table (2). The lattice strain (ε) is measured using Eq. (3) [29].

$$\varepsilon = \beta/4\tan(\theta) \tag{3}$$

The crystallite size (D) of samples was impacted and increased with increasing the SiO_2 nanoparticles in the core–shell structure at the matrix. Where D was improved from 12.25 to 19.44 nm. Additionally, the (ε) demonstrated influence by the contribution of the core–shell nanoparticles, as shown in Table (2).

FTIR spectroscopy was used to investigate the samples' surface to understand the formation of the PVA-UHMWPEO blended polymer and PVA-UHMWPEO/Ag@SiO_2 nanocomposite, as shown in Fig. 2. The FTIR spectrum of samples presented several absorption peaks in the range of 4000–500 cm^{-1} wavenumber that verifies the formation of the PVA-UHMWPEO/Ag@SiO_2 nanocomposite. Blended polymers spectrum exhibited strong absorption peaks a 3347, 2897, 1732, 1450, 1242, 1109, 0947, 0843, and 0611 cm^{-1} linked to O–H bond, C-H symmetric stretch, C = O bond, CH_2, O–H bond, C–O–C stretching of an acetyl group, C-O bond, C-H bond, and C-O bond, respectively. Presenting bands represented the combination and overlap of both polymers, which refers to a formulation of the strong interaction between polymers in agreement with the literature [5, 30].

FTIR spectrum was efficiently impacted by the nanoparticles that showed a strong bond of the silica network, where

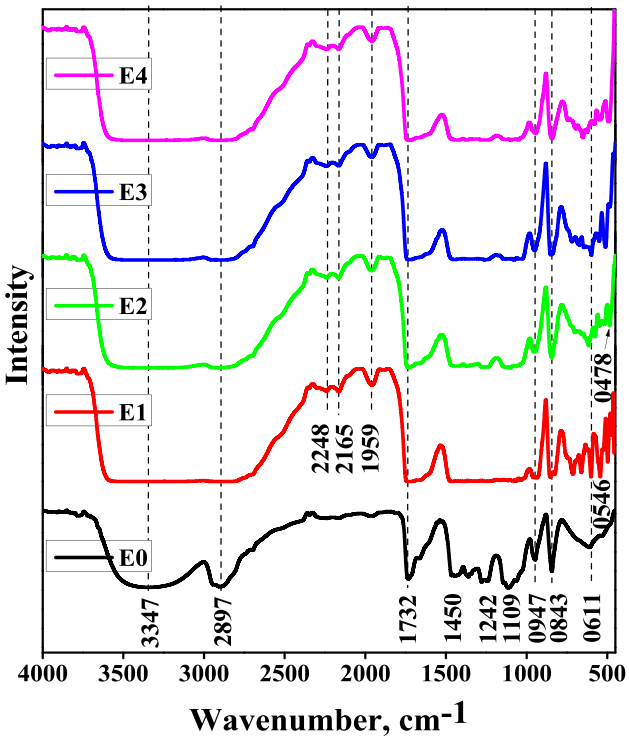

Fig. 2 FTIR spectrum of prepared samples

broad absorption peaks between 3590 and 2707 cm^{-1} correspond to the (O–H) bending vibrations. Other new absorption peaks located at 2248 and 2156 cm^{-1} were associated with (C≡C) stretching vibration of alkyne groups [17], and 1959 cm^{-1} was associated with (N–H) stretching vibration in the presence of the (NH3+) group [19]. Other peaks related to SiO_2 were diapered, such as 1450 cm^{-1} formulation of silanol (Si–OH) groups [18], 1109 cm^{-1} of (Si–O–Si) symmetrical stretching [19], 0947 cm^{-1} of (Si–OH) bending vibration [25], 0843 cm^{-1} of (O–Si–O) bending vibration [19] and 0478 cm^{-1} rocking vibration of (Si–O–Si) bending [22, 31]. The presence of Ag in PVA-UHMWPEO/Ag@SiO_2 nanocomposite depicted at the absorption peaks at 530 cm^{-1} attributed to (Ag–O) stretching [18, 32]. Ag represented an absorption band below 1000 cm^{-1} that indicates the pure form of Ag instead of silver oxides [19]. The FTIR spectrum of the PVA-UHMWPEO/Ag@SiO_2 nanocomposite exhibited several new absorption peaks, such as 478 cm^{-1} of (Si–O) rocking vibration and 0947 cm^{-1} of (Si–OH) asymmetric vibration that reflected the product of silica network as Ag@SiO_2 core–shell nanoparticles in strong agreement with the literature [19].

3.2 Morphological Study

Fig. 3 visualizes the OLM images with 40X magnification of PVA-UHMWPEO and PVA-UHMWPEO/Ag@SiO_2 NCFs. OLM images of samples are presented in Figure 3 (E0, E1, E2, E3, and E4). PVA-UHMWPEO films showed a clear image with a fine homogeneous polymer matrix. The incorporation of Ag@SiO_2 NPs showed changes in the surface morphology and presented a formulation of spherical shapes on the surface. The nanoparticles do not affect the optical transparency of the nanocomposites. Interestingly, increasing the NPs concentration is associated with gradually developing these spherical to core-shell shapes at 0.045 wt. %. This behavior developed to present core-shell NPs at 0.060 wt. %, these results matched another finding by the researcher's prepared Ag@SiO_2 core-shell NPs [19].

FESEM was employed to confirm the finding, where the surface morphology of blended polymers and nanocomposites was examined on the sample surface (left side) and FESEM-EDX (right side), as shown in Figure 4. The blended polymer films exhibited a homogeneous, grainy, rough surface morphology. Ag@SiO_2 nanoparticles significantly impacted the polymer matrix and displayed good dispersion and granular structure without aggregations. Increasing the loading ratio of Ag@SiO_2 nanoparticles revealed formalizing spherical shapes; meanwhile, the higher percentages of SiO_2 nanoparticles of 0.045 and 0.060 wt. % in the matrix indicated a clear formulation of core-shell shapes in these samples, as shown in Figure 3 (E3 and E4).

The difference in the distinct boundary between the amorphous SiO_2 and the crystalline Ag NPs that utilize the SiO_2 NPs to grow and surround a shell of the well-dispersed Ag NPs. This behavior is clearly presented in Figures 3 and 4 in both OLM and FESEM images. Where the significant difference in electron density between the core and shell helped to present the core-shell spherical shape as reported by literature [18, 19], they prepared Ag@SiO_2 core-shell nanoparticles that particles are uniform and nearly spherical with the 14 nm size of Ag core and 8 nm size of SiO_2 shell.

The FESEM in Figure 4 matches the OLM images in Figure 3 and strongly supports the FTIR finding in Figure 2, which reveals this formalization in agreement with other research reports [18, 19]. The average particle size of the nanoparticles presented in the SEM images is to be a few nm to 1 μm in all the samples, as shown in Figure 4. Whereas the EDX images presented the clear core shell formulation with a size that matched the optical microscopy images, where the size of Ag cores was calculated to be between 20 nm to 190 nm surrounded by the SiO_2 shells between 20 nm to more than 600 nm, as shown in Figures 4 and 3 E2 to E4. In addition, the EDX results confirmed the weight present of the element of Ag and SiO_2, as shown in the table in Figure 4. In comparison, the crystalline size was calculated for the samples using the Scherer formula (2) that presented increasing in the particle size (D) of the samples with increasing the SiO_2 loading ratio and formulation of Ag@SiO_2 nanostructure as shown in Table 2. The XRD and OM images strongly support these SEM and EDX results.

3.3 Optical Properties

Figure 5 revealed the UV/Visible absorption spectra and absorption coefficient of blended polymer, and different loading ratios of Ag@SiO_2 core–shell nanoparticles were characterized in the region (200–1200) nm. PVA-UHMWPEO blended polymer (E0) exhibited absorption peaks at 200 nm. This strong absorption peak transition could cause by the covalent bonding or plasmonic π-π* stacking, which is the primary interaction between the blended polymers. The contribution of Ag@SiO_2 core–shell nanoparticles resulted in a small peak shoulder at 280 nm, which was not presented in (E0), which is conjunctive to the n-π* (C=O) transition [5]. Increasing the reaction time is associated with shifting the plasmonic peak from 200 to 280 nm. Moreover, increasing the number of carbon atoms sp^2 hybridized is attributed to this shifting [10].

The absorption behavior was significantly increased after increasing the concertation of the nanoparticles. The Ag@SiO_2 core–shell nanoparticle's contribution significantly impacts the absorption behavior of all the nanocomposites compared with the blended polymers (E0). Interestingly, at 200 nm, absorption behavior was improved considerably after increasing the concentration of core–shell nanoparticles from 1.744 of E0 to 3.479, 3.53, 3.716, and 3.873 for

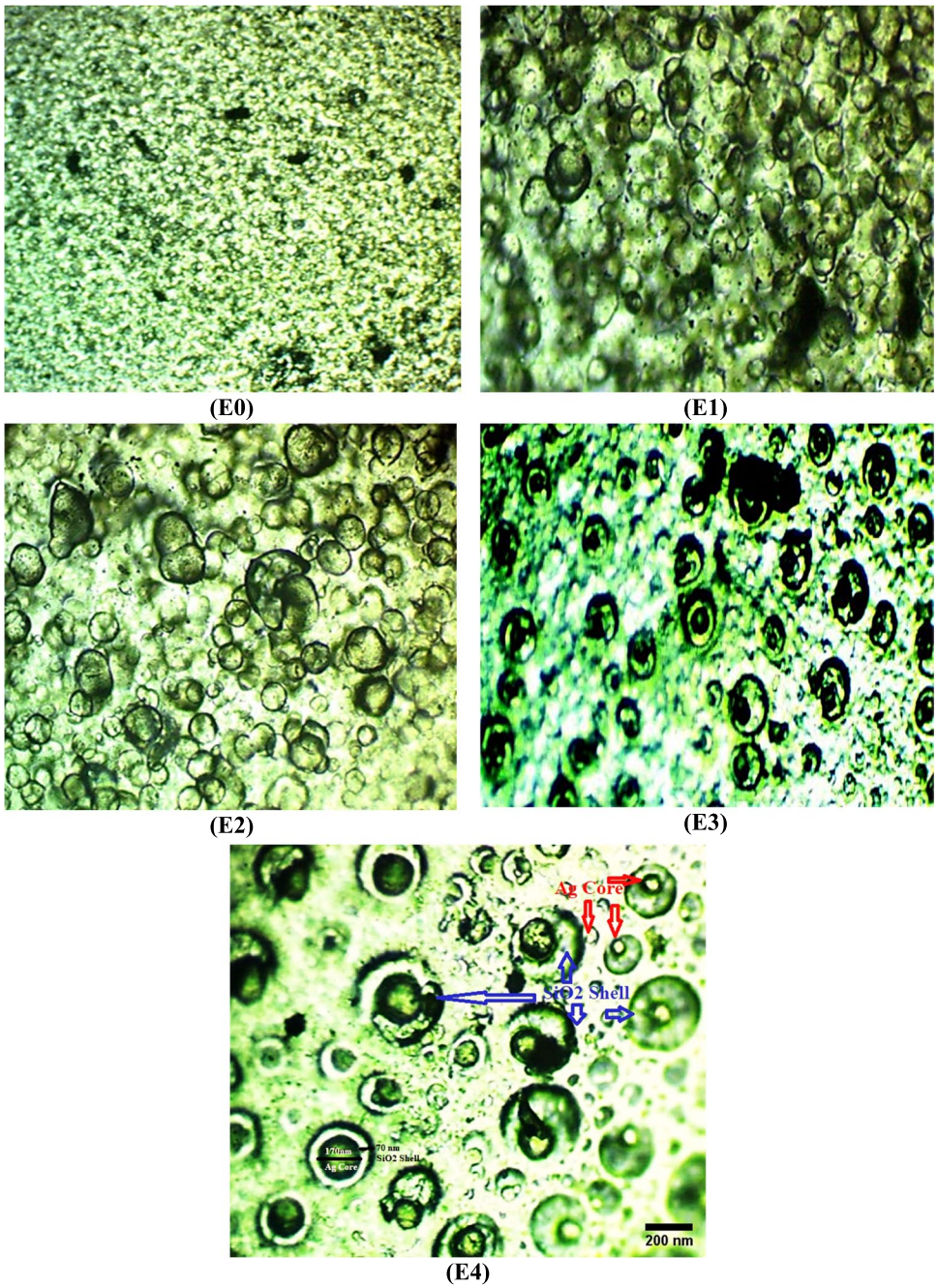

Fig. 3 OLM images of samples

E1, E2, E3, and E4, respectively; this confirms the complexation between the blend polymers and $Ag@SiO_2$ core–shell nanoparticles [33], as presented in Fig. 5 (a).

The optical energy gap of samples was calculated from the interception of the extrapolated linear component and the photon energy using the flowing Eq. (4) [34].

$$ahv = B(hv - Eg)^r \tag{4}$$

where (hυ) at $(\alpha h\nu)^{1/n} = 0$, *(B)* is constant, (*h*) is Planck's constant, (*v*) frequency, (E_g) the energy of phonon, and (r) the exponential constant, which represent in various values depending on the transition formulation. For instance, the (r) value is 1/2 and 3/2 for allowed and forbidden direct or 2 and 3 for indirect transitions, respectively [10, 35]. The differences between $(\alpha h\upsilon)^{1/2}$ absorption edges as functional of the incident photon energy of the samples are presented in Fig. 5 (b). The indirect optical gap (Eg) calculated in Fig. 5, a liner was drawn from the plot between $(\alpha h\upsilon)^{1/2}$ and the photon energy $(\alpha h\upsilon)^{1/2}$. The blended polymers E0 showed indirect transition with band gap 5.0 eV, whereas the impact of $Ag@SiO_2$ core–shell nanoparticles was associated with

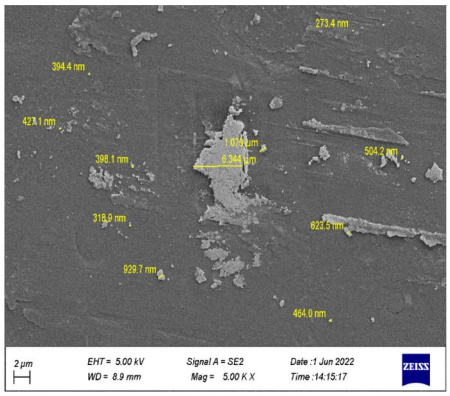

(E0)

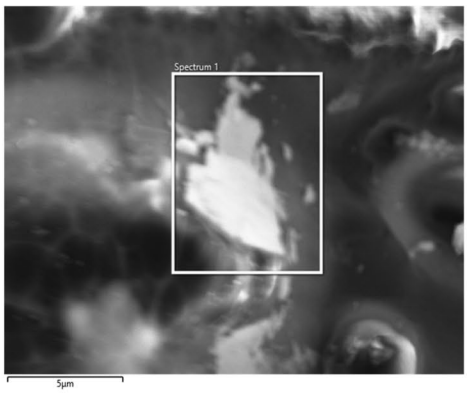

(E0)

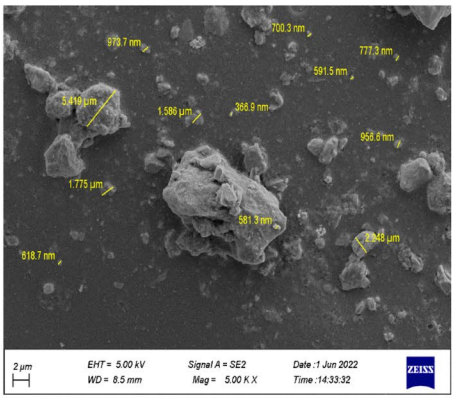

(E1)

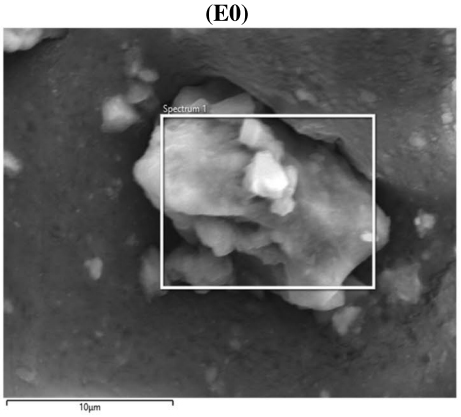

(E1)

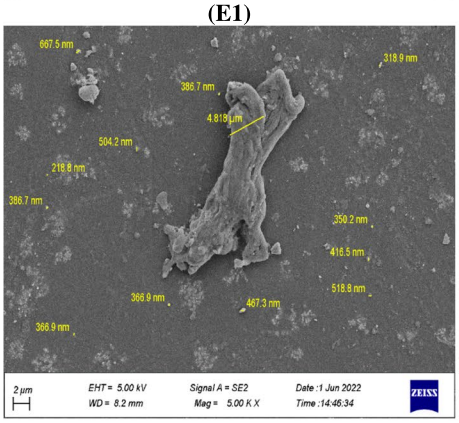

(E2)

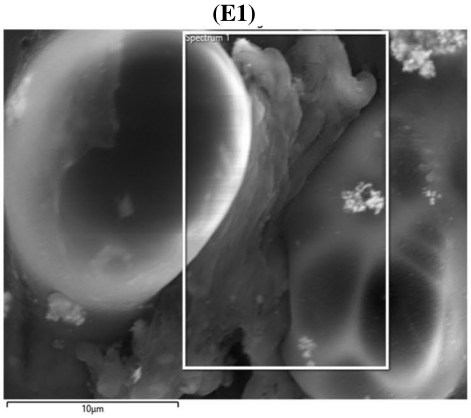

(E2)

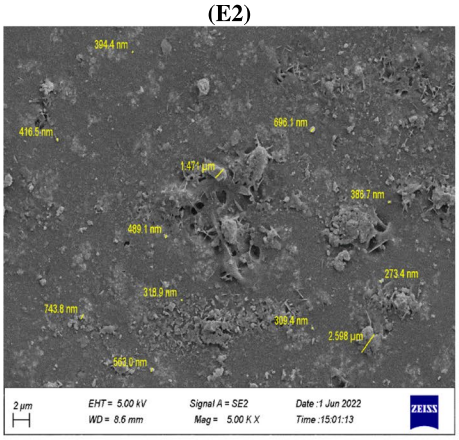

(E3)

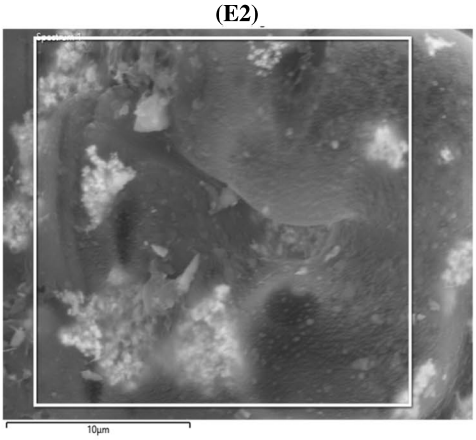

(E3)

Fig. 4 FESEM, FESM-EDX elements (left side) and images (right side) of samples.

Fig. 4 (continued)

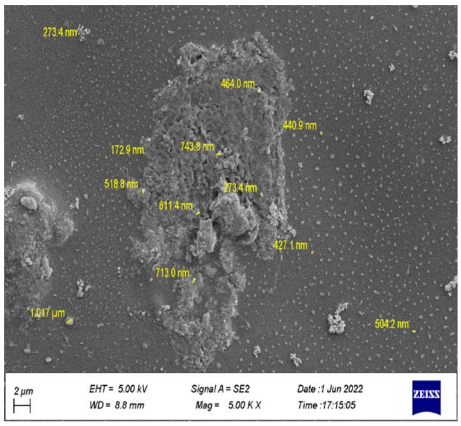

(E4)

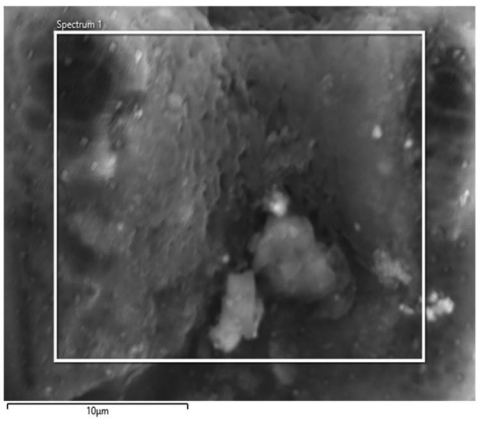

(E4)

Element	Line Type	Weight %	Weight %	Atomic %
C	K	63.21	0.49	70.66
O	K	33.61	0.48	28.20
Si	K	0.98	0.05	0.47
Ag	L	1.28	0.13	0.16
Na	K	0.55	0.06	0.32
Al	K	0.37	0.04	0.18

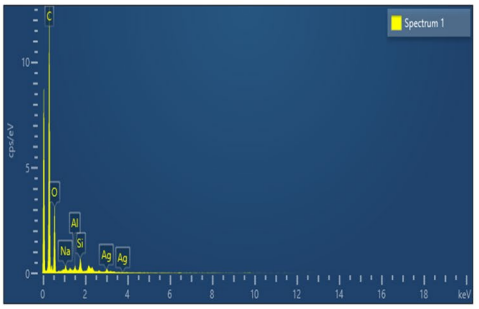

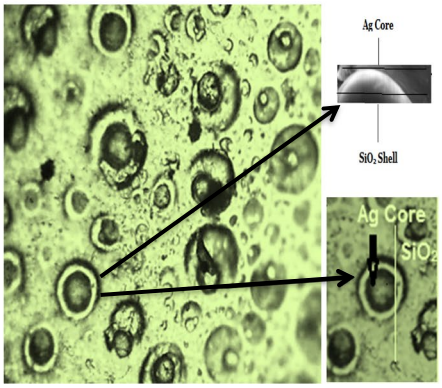

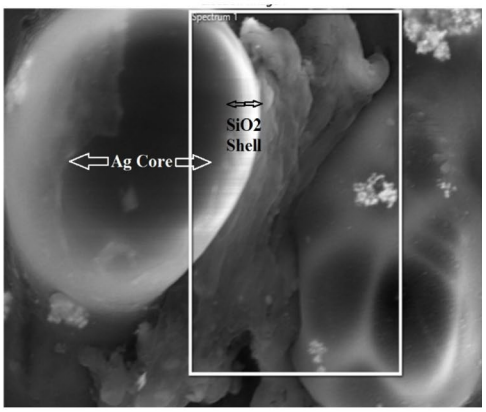

this notable improvement. Increasing the loading ratio of the higher ratio Ag@SiO_2 core–shell revealed an exciting reduction in the band gap up to 4.0 eV of E4, which had a higher percentage of NPs. Because of the polarization effects, the dielectric constant and dielectric loss were gradually reduced with increasing frequency and reached constant values at higher frequencies [24]. The high potential of electron transfer is enhanced by increasing the SiO_2 nanoparticle concentration, associated modifications in the structure of the additional NPs, and reducing the band gap due to the interaction between the blended polymer and Ag@SiO_2 core–shell nanoparticle. Where, Ag@SiO_2 core–shell associates of localized states that produced complexes charge transfer between the lowest unoccupied molecular orbital (LUMO) and the highest occupied molecular orbital (HOMO) [33], these results could significantly be used for a new generation of the optoelectronic device.

3.4 AC Electrical Properties

Dielectric constant and loss factors are the most convenient and efficient methods of studying the structure of polymers [36]. The electrical conductance of insulating polymer materials can improve by adding a specific conductive filler [37]. Dielectric constant can define as "the ratio between the capacitance of a capacitor containing an insulator material between its conducting plates to the capacity of the same size with a vacuum between the insulator plates [38].

Table 2 Summarized the diffraction angle, d-spacing, FWHM (β), crystallite size (D), average crystallite size, and the average lattice strain of blended polymers and nanocomposite

Samples	2θ (˚)	d (nm)	β (˚)	D (nm)	Average crystallite size (nm)	Average lattice strain* 10^{-3}
E0	18.767	0.47244	1.012	8	12.25	7.189
	22.782	0.39001	0.811	10		
	28.76	0.31016	0.418	20		
	39.252	0.22933	0.751	11		
E1	18.869	0.4699	0.898	9	16.83	3.344
	23.013	0.38614	0.679	12		
	29.077	0.30685	0.374	22		
	30.513	0.29272	0.318	27		
	37.958	0.23685	0.398	21		
	39.161	0.22984	0.595	14		
	42.815	0.21104	0.454	19		
	44.119	0.2051	0.618	14		
	47.169	0.19252	0.53	16		
	48.207	0.18861	0.484	18		
	64.393	0.14457	0.696	13		
	77.163	0.12352	0.587	17		
E2	18.977	0.46727	0.858	9	16.9	3.543
	23.143	0.38401	0.905	9		
	28.817	0.30956	0.322	26		
	37.891	0.23725	0.452	19		
	42.632	0.2119	0.369	24		
	44.027	0.2055	0.568	15		
	46.995	0.1932	0.535	16		
	48.029	0.18927	0.397	22		
	64.229	0.1449	0.725	13		
	77.205	0.12346	0.645	16		
E3	19.038	0.46577	1.055	7	16.5	3.709
	23.151	0.38388	0.971	8		
	29.028	0.30735	0.358	23		
	38.023	0.23646	0.354	24		
	39.06	0.23042	0.484	17		
	40.408	0.22303	0.816	10		
	42.78	0.2112	0.463	18		
	44.255	0.2045	0.558	15		
	47.16	0.19256	0.433	20		
	48.185	0.1887	0.391	23		
	64.405	0.14454	0.443	21		
	77.338	0.12328	0.815	12		
E4	18.763	0.47254	0.923	8	19.44	3.875
	22.663	0.39204	0.73	11		
	29.009	0.30756	0.338	25		
	30.516	0.2927	0.347	24		
	35.594	0.25202	0.482	17		
	39.052	0.23046	0.429	20		
	42.807	0.21107	0.381	23		
	47.156	0.19257	0.459	19		
	48.196	0.18865	0.324	28		

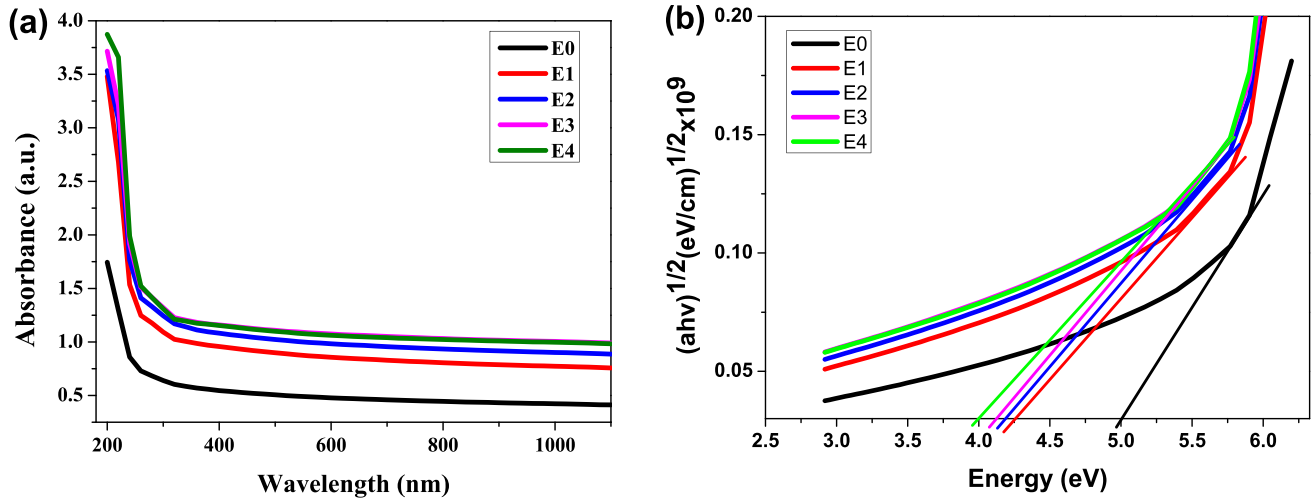

Fig. 5 Optical characteristics of prepared films

$$\varepsilon' = C_p/C_o \tag{5}$$

C_p and C_o mean the capacitor has an insulator material and vacuum, respectively. The (ε'') or dielectric loss is given by formula (6) [39].

$$\varepsilon'' = \acute{\varepsilon} D'' \tag{6}$$

Where (D) explains the coefficient of dispersion.

Figure 6 (a, and b) shows the results of ($\acute{\varepsilon}$) and (ε'') with frequency (f) at RT. All the effects were reduced with increasing frequency. However, the nanocomposites revealed higher values than blended polymer E0. Alternating conductivity is a function used for the existence of alternating potential that could represent the dissipated power in the insulator. The electrical conductivity was computed by Eq. (7) [39].

$$\sigma_{AC} = \omega\, \varepsilon_o\, \varepsilon'' \tag{7}$$

In the insulating material, σ_{AC} calculates the generated temperature, which results from the rotation of the dipole in their positions [40]. ω means the applied filed angular frequency ($\omega = 2\pi f$). Because of the existence of dipole moments (μ) having enough or suitable time in these regions to order themselves in the direction of the applied electrical field (E), both $\acute{\varepsilon}$ and ε''have high values at low (f) values. More ions cannot propagate in the direction of E because the dielectric properties of the charge carriers (particles or holes) become less effective. This behavior emphasizes non-Debye activity for polymer electrolytes. That cannot obey the field separation at high f values due to a lack of time [41]. Both $\acute{\varepsilon}$ and ε'' decreased with the increase of Ag@SiO_2 core–shell nanoparticles loading ratio. This result may improve the σ_{AC} due to increased PC density [39]. Figure 6 (c) depicts the σ_{AC} variations of PVA-UHMWPEO/ Ag@SiO_2 nanocomposites with f. This behavior can be attributed to the interfacial P of the electrical conductivity with increasing the f value [42]. σ_{AC} values were enhanced from $9.6*10^{-9}$ to $35.69*10^{-9}$ $S.cm^{-1}$ at $5*10^{-6}$ Hz with the increasing Ag@SiO_2 core–shell nanoparticle contents due to the increase in the density of charge carriers, which could promise optoelectronic application [41, 43].

Moreover, mixing different polymers creates more complex sites and increases the number of ion migrations, which improves ionic conductivity [44]. PEO, PVA, and PVP are artificial polar polymer that develops proton-conducting samples [45]. According to the nature of the polar polymers, they have been utilized to create proton-conducting electrolyte films [46]. However, these polymers can significantly reform their structural, electrical, thermal, and mechanical properties when doped with different inorganic and organic acids or salt dopants [47]. Therefore, the ionic conductivity of these blended polymers could boost and able modulate the ionic conductivity with doping oxide as nanocomposites such as graphene, CNTs, silicon, and nano-metal oxide, etc., resulting in polymer-based electrolytes [45].

The Ag and SiO_2 NPs absorbed the incident photons associated with exciting the electron in the valance band to move to the conductive band of SiO_2. Meanwhile, the VB generates the hole with the same amount of excited electrons. However, partially excited electron transfer from a conductive band of SiO_2 to the Ag NPs surface because the Fermi energy level of SiO_2 is higher than of Ag metal. When Ag and SiO_2 NPs form a core–shell structure, free electrons migrate from the Fermi level of metallic Ag to the conductive band of SiO_2 to reach an equilibrium Fermi state. This behavior leads to the depletion layer formation and an internal electrical field at the interface. The electron migrates

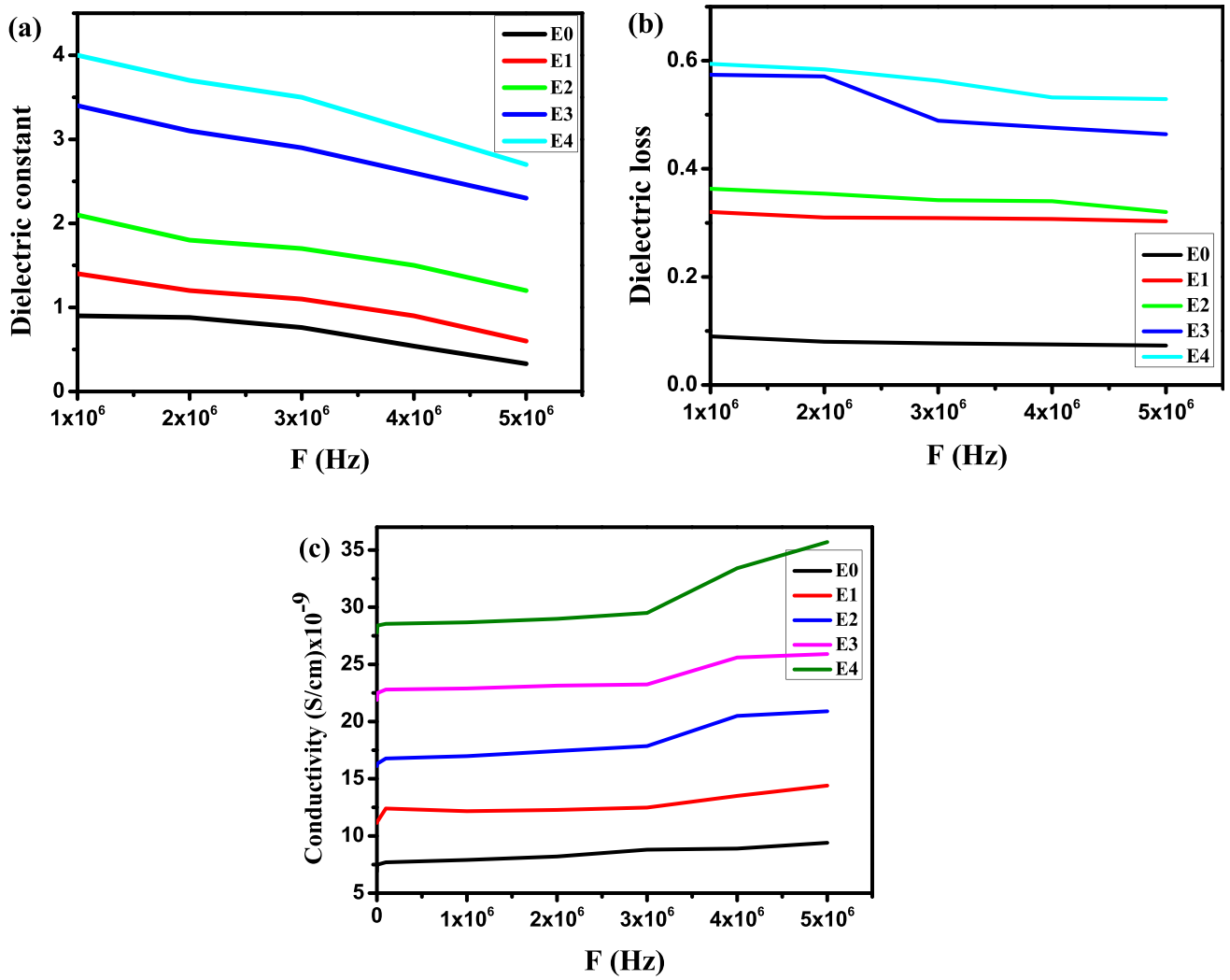

Fig. 6 AC characteristics of prepared films

away from the depleted region, which causes the creation of excess positive and negative charges on the surface of both Ag and SiO_2 nanoparticles, respectively. The internal electrical field is directly transferred from Ag toward the SiO_2 NP [18]. Moreover, the Ag@SiO_2 composite absorbs light near-ultraviolet–visible light, which assists in absorbing more photons and leads to a more exciting electron within SiO_2, as shown in Fig. 5.

The contact between Ag and SiO_2 surfaces as core–shell resulted in an electron that enhanced the area in their interface. This effectively facilitates the electron's uptake and then increases the conductivity. These reactions were increased due to the formation of core–shell between the Ag and SiO_2 due to the intense local electric field close to the surface of nanoparticles, as shown in Fig. 6. On the other hand, the interaction with the electron in a core–shell structure is signified by the electron transition from occupied to unoccupied states in the band structure. Where the occupied states are below the Fermi level, the unoccupied states are mostly above the Fermi level. Increasing the SiO_2 ratio led to the formulation of core–shell structure in samples that enhanced charge carrier numbers through the generated electric field, as exhibited in Fig. 6-E4. Fewer free carriers in nanocomposites could be ignored compared with the conductivity produced by polarization, which could be the possible reason.

This result agreed with the same behavior of literature [48]; they used PVDF flexible polymer as substrate and studied the impact of reinforced with fabricated fillers Ag@SiO_2 nanoparticles core–shell structure. Their results indicate a correlation between the dielectric constant and dielectric loss of nanocomposites with the filler's contents. The dielectric constant of composites increases from 8.42 to 10.1 after increasing the content of the filler from 5 to 20 wt%. Whereas it decreased with increasing the frequency of the test due to the dielectric relaxation of dielectrics,

the dielectric loss of the samples had a similar behavior of PVDF polymer that decreased first and then increased with the increase of frequency. Also, the conductivity of nanocomposites is increased with the increase in frequency. This result strongly agrees with the behavior results of this investigation.

4 Conclusions

The bimetallic $Ag@SiO_2$ core–shell nanoparticles were successfully prepared using a green acoustic-sonication method to fabricate new PVA-UHMWPEO/$Ag@SiO_2$ NCFs. FTIR analysis revealed strong interfacial interaction and hydrogen bonds between the matrix components without affecting the crystalline behavior of the materials, as shown by XRD. OLM and FESEM exhibited the composition of $Ag@SiO_2$ core–shell nanoparticles with fine homogenate and good dispersion in the matrix. Increasing the loading ratio of the $Ag@SiO_2$ core–shell exposed a significant change in the optical behavior. The absorption peaks were improved from 1.75 to 3.91 at 200 nm wavelength optical bandgap (E_g) values decreased from 5 to 4 eV. Meanwhile, the electrical characterization showed improved dielectric and conductivity, which increased from $9.6*10^{-9}$ to $35.69*10^{-9}$ $S.cm^{-1}$. These results could interest optoelectronic devices and membrane transistors as a high-k layer.

Acknowledgements The authors would like to thank the department of physics, university of Babylon, Iraq, for their support.

Authors' Contributions Ehssan Al-Bermany designed, wrote, and analyzed the FTIR, XRD, SEM, and OML and improved and reviewed the paper. Ali Tao'mah Mekhalif performed all the experiments, and Hikmat A Banimuslem performed and wrote the experiments and contributed to the introduction section. Karar Abdali contributed to the optical properties and data examination, and Mohammed M. Sabri analyzed the electrical properties of the research and data examination. All authors read and approved the final manuscript.

Funding No funding applied.

Data Availability The data are available in the manuscript.

Declarations

Competing interests The authors declare no competing interests.

Ethics Approval Not applicable.

Consent to Participate Not applicable.

Consent for Publication Not applicable.

Conflict of Interest The authors declare that they have no conflict of interest.

References

1. Smith RC, Liang C, Landry M et al (2008) The mechanisms leading to the useful electrical properties of polymer nanodielectrics. IEEE Trans Dielectr Electr Insul 15:187–196. https://doi.org/10.1109/T-DEI.2008.4446750
2. Tanaka T, Vaughan AS (2022) Tailoring of nanocomposite dielectrics : from fundamentals to devices and applications. 441. https://doi.org/10.1201/9781315201535
3. Abdali K Structural, Morphological, and Gamma Ray Shielding (GRS) Characterization of HVCMC/PVP/PEG Polymer Blend Encapsulated with Silicon Dioxide Nanoparticles. Silicon 1–6 (2022). https://doi.org/10.1007/s12633-022-01678-8
4. Abdelamir AI, Al-Bermany E, Hashim FS Important factors affecting the microstructure and mechanical properties of PEG/GO-based nanographene composites fabricated applying assembly-acoustic method. In: AIP Conference Proceedings. p 020110 (2020)
5. Aldulaimi NR, Al-Bermany E (2022) Tuning the bandgap and absorption behaviour of the newly-fabricated Ultrahigh Molecular weight Polyethylene Oxide- Polyvinyl Alcohol/ Graphene Oxide hybrid nanocomposites. Polym Polym Compos 30:096739112211121. https://doi.org/10.1177/09673911221112196
6. Chaudhary P, Fatima F, Kumar A (2020) Relevance of Nanomaterials in Food Packaging and its Advanced Future Prospects. J Inorg Organomet Polym Mater 30:5180–5192. https://doi.org/10.1007/s10904-020-01674-8
7. Menazea AA, Ismail AM, Awwad NS, Ibrahium HA (2020) Physical characterization and antibacterial activity of PVA/Chitosan matrix doped by selenium nanoparticles prepared via one-pot laser ablation route. J Market Res 9:9598–9606. https://doi.org/10.1016/j.jmrt.2020.06.077
8. Abd El-Kader MFH, Elabbasy MT, Ahmed MK, Menazea AA (2021) Structural, morphological features, and antibacterial behavior of PVA/PVP polymeric blends doped with silver nanoparticles via pulsed laser ablation. J Market Res 13:291–300. https://doi.org/10.1016/j.jmrt.2021.04.055
9. El-Kader MFHA, Elabbasy MT, Adeboye AA, Menazea AA Nanocomposite of PVA/PVP blend incorporated by copper oxide nanoparticles via nanosecond laser ablation for antibacterial activity enhancement. Polymer Bulletin 1–18 (2021). https://doi.org/10.1007/s00289-021-03975-5
10. Kadhim MA, Al-Bermany E (2021) New fabricated PMMA-PVA/graphene oxide nanocomposites: Structure, optical properties and application. J Compos Mater 55:2793–2806. https://doi.org/10.1177/0021998321995912
11. Menazea AA (2020) One-Pot Pulsed Laser Ablation route assisted copper oxide nanoparticles doped in PEO/PVP blend for the electrical conductivity enhancement. J Market Res 9:2412–2422. https://doi.org/10.1016/j.jmrt.2019.12.073
12. Ghazi RA, Al-Mayalee KH, Al-Bermany E et al (2022) Impact of polymer molecular weights and graphene nanosheets on fabricated PVA-PEG/GO nanocomposites: Morphology, sorption behavior and shielding application. AIMS Materials Science 9:584–603. https://doi.org/10.3934/matersci.2022035
13. Abdali K (2022) Synthesis, characterization and USW sensor of PEO/PMMA/PVP doped with zirconium dioxide nanoparticles. Trans Electr Electron Mater. https://doi.org/10.1007/s42341-022-00388-7
14. Cao G, Brinker CF (2008) Annual Review of. Nano Res 1:645
15. Bigg DM (1979) Mechanical, thermal, and electrical properties of metal fiber-filled polymer composites. Polym Eng Sci 19:1188–1192. https://doi.org/10.1002/pen.760191610
16. Szabo A (1984) Theory of fluorescence depolarization in macromolecules and membranes. J Chem Phys 81:150–167. https://doi.org/10.1063/1.447378

17. Hamida RS, Abdelmeguid NE, Ali MA et al (2020) Synthesis of Silver Nanoparticles Using a Novel Cyanobacteria Desertifilum sp. extract: Their Antibacterial and Cytotoxicity Effects. Int J Nanomed 15:49–63. https://doi.org/10.2147/IJN.S238575
18. Assis M, Simoes LGP, Tremiliosi GC et al (2021) Sio2-ag composite as a highly virucidal material: A roadmap that rapidly eliminates sars-cov-2. Nanomaterials 11:1–19. https://doi.org/10.3390/nano11030638
19. Sakthisabarimoorthi A, Martin Britto Dhas SA, Jose M (2018) Nonlinear optical properties of Ag@SiO2 core-shell nanoparticles investigated by continuous wave He-Ne laser. Mater Chem Phys 212:224–229. https://doi.org/10.1016/j.matchemphys.2018.03.047
20. Asselin J, Legros P, Grégoire A, Boudreau D (2016) Correlating Metal-Enhanced Fluorescence and Structural Properties in Ag@SiO2 Core-Shell Nanoparticles. Plasmonics 11:1369–1376. https://doi.org/10.1007/s11468-016-0186-5
21. Wang J, White WB, Adair JH (2010) Optical properties of core–shell structured Ag/SiO2 nanocomposites. Mater Sci Eng, B 166:235–238. https://doi.org/10.1016/j.mseb.2009.11.026
22. Liang Y, Ouyang J, Wang H et al (2012) Synthesis and characterization of core-shell structured SiO 2 @YVO 4: Yb 3+, Er 3+ microspheres. Appl Surf Sci 258:3689–3694. https://doi.org/10.1016/j.apsusc.2011.12.006
23. Das MR, Sarma RK, Saikia R et al (2011) Synthesis of silver nanoparticles in an aqueous suspension of graphene oxide sheets and its antimicrobial activity. Colloids Surf, B 83:16–22. https://doi.org/10.1016/j.colsurfb.2010.10.033
24. Gün Gök Z (2022) Synthesis and characterization of polyvinyl alcohol–silk sericin nanofibers containing gelatin-capped silver nanoparticles for antibacterial applications. Polym Bull 166:235–238. https://doi.org/10.1007/s00289-022-04455-0
25. Sakthisabarimoorthi A, Jose M, Martin Britto Dhas SA, Jerome Das S (2017) Fabrication of Cu@Ag core–shell nanoparticles for nonlinear optical applications. J Mater Sci: Mater Electron 28:4545–4552. https://doi.org/10.1007/s10854-016-6090-0
26. Al-shammari AK, Al-Bermany E (2022) Polymer functional group impact on the thermo-mechanical properties of polyacrylic acid, polyacrylic amide- poly (vinyl alcohol) nanocomposites reinforced by graphene oxide nanosheets. J Polym Res 29:351. https://doi.org/10.1007/s10965-022-03210-3
27. Kandulna R, Choudhary RB (2018) Concentration-dependent behaviors of ZnO-reinforced PVA–ZnO nanocomposites as electron transport materials for OLED application. Polym Bull 75:3089–3107. https://doi.org/10.1007/s00289-017-2186-9
28. Yang Z, Zhang Y, Wen B (2019) Enhanced electromagnetic interference shielding capability in bamboo fiber@polyaniline composites through microwave reflection cavity design. Compos Sci Technol 178:41–49. https://doi.org/10.1016/j.compscitech.2019.04.023
29. Qiu M, Zhang Y, Wen B (2018) Facile synthesis of polyaniline nanostructures with effective electromagnetic interference shielding performance. J Mater Sci: Mater Electron 29:10437–10444. https://doi.org/10.1007/s10854-018-9100-6
30. Cao Y-C, Xu C, Wu X et al (2011) A poly (ethylene oxide)/graphene oxide electrolyte membrane for low temperature polymer fuel cells. J Power Sources 196:8377–8382. https://doi.org/10.1016/j.jpowsour.2011.06.074
31. Ramalla I, Gupta RK, Bansal K (2015) Effect on superhydrophobic surfaces on electrical porcelain insulator, improved technique at polluted areas for longer life and reliability. Inter J. of Eng & Techol 4:509
32. Oje AI, Ogwu AA, Mirzaeian M, Tsendzughul N (2018) Electrochemical energy storage of silver and silver oxide thin films in an aqueous NaCl electrolyte. J Electroanal Chem 829:59–68. https://doi.org/10.1016/j.jelechem.2018.10.001
33. Gaabour LH (2019) Influence of silica nanoparticles incorporated with chitosan/polyacrylamide polymer nanocomposites. J Market Res 8:2157–2163. https://doi.org/10.1016/j.jmrt.2019.02.003
34. Pankove JI, Kiewit DA (1972) Optical Processes in Semiconductors. J Electrochem Soc 119:156C. https://doi.org/10.1149/1.2404256
35. Hussein AM, Dannoun EMA, Aziz SB et al (2020) Steps toward the band gap identification in polystyrene based solid polymer nanocomposites integrated with tin titanate nanoparticles. Polymers 12:1–21. https://doi.org/10.3390/polym12102320
36. Ji KA, Design M, Chemistry A (1998) Electrical properties of poly (n-butylamino). J Mater Sci 3:2955–2959
37. Shekhar S, Prasad V, Subramanyam SV (2006) Structural and electrical properties of composites of polymer-iron carbide nanoparticles embedded in carbon. Mater Sci and Eng B: Solid-State Mater for Adv Technol 133:108–112. https://doi.org/10.1016/j.mseb.2006.06.010
38. Hayany AT (1970) Solid dielectric waveguide filters
39. Hu H, Zhang F, Luo S et al (2020) Recent advances in rational design of polymer nanocomposite dielectrics for energy storage. Nano Energy 74:104844. https://doi.org/10.1016/j.nanoen.2020.104844
40. Tareev BM, Tareev BM (1979) Physics of Dielectric Materials. Mir Publ, Moscow, p 90
41. Al-Abbas SS, Ghazi RA, Al-shammari AK et al (2021) Influence of the polymer molecular weights on the electrical properties of Poly(vinyl alcohol) – Poly(ethylene glycols)/Graphene oxide nanocomposites. Mater Today Proc 42:2469–2474. https://doi.org/10.1016/j.matpr.2020.12.565
42. Coetzee D, Venkataraman M, Militky J, Petru M (2020) Influence of nanoparticles on thermal and electrical conductivity of composites. Polymers 12, https://doi.org/10.3390/POLYM12040742
43. Abdali K (2022) Structural, optical, electrical properties, and relative humidity sensor application of PVA/Dextrin polymeric blend loaded with silicon dioxide nanoparticles. J Mater Sci: Mater Electron 33:18199–18208. https://doi.org/10.1007/s10854-022-08676-x
44. Hezma AM, Elashmawi IS, Rajeh A, Kamal M (2016) Change Spectroscopic, thermal and mechanical studies of PU/PVC blends. Physica B 495:4–10. https://doi.org/10.1016/j.physb.2016.04.043
45. Patla SK, Mukhopadhyay M, Ray R (2019) Ion specificity towards structure-property correlation of poly (ethylene oxide) [PEO]-NH 4 I and PEO-KBr composite solid polymer electrolyte. Ionics 25:627–639. https://doi.org/10.1007/s11581-018-2711-3
46. Buraidah MH, Teo LP, Majid SR, Arof AK (2009) Ionic conductivity by correlated barrier hopping in NH4I doped chitosan solid electrolyte. Physica B 404:1373–1379. https://doi.org/10.1016/j.physb.2008.12.027
47. Prajapati GK, Roshan R, Gupta PN (2010) Effect of plasticizer on ionic transport and dielectric properties of PVAH3PO4 proton conducting polymeric electrolytes. J Phys Chem Solids 71:1717–1723. https://doi.org/10.1016/j.jpcs.2010.08.023
48. Weng L, Wang X, Zhang X et al (2020) The effect of Ag@SiO2 core-shell nanoparticles on the dielectric properties of PVDF based nanocomposites. Polym Compos 41:2245–2253